Supplementary Information for

# Structural transformations with $Li^+$-deintercalation in cathode materials $Li_3VSc(PO_4)_3$ with *anti*-NASICON and NASICON structures

Tatyana I. Perfilyeva, [a] Anastasia M. Alekseeva,*[a] Andrey V. Mironov, [a] Artem A. Kabanov, [b] Maxim V. Zakharkin, [a] Ivan V. Mikheev, [a] Andrey P. Marenko, [a] Artem V. Marikutsa, [a] Alexey V. Tkachev, [c] Sergey V. Zhurenko,[c] Andrey A. Gippius, [ac] Anna E. Medvedeva, [d] Alexander E. Baranchikov, [d] Oleg A. Drozhzhin [ae] and Evgeny V. Antipov [ae]

[a] *Lomonosov Moscow State University, Moscow 119991, Russia. E-mail: alekseevaam@gmail.com*

[b] *P.N. Lebedev Physical Institute of the Russian Academy of Sciences, Samara 443011, Russia*

[c] *Lebedev Physical Institute of Russian Academy of Sciences, Moscow 119991, Russia*

[d] *Kurnakov Institute of General and Inorganic Chemistry of Russian Academy of Sciences, Moscow 119991, Russia*

[e] *Skolkovo Institute of Science and Technology, Moscow 143026, Russia*

**Contents**

**Section 1**. Microstructural characterization.

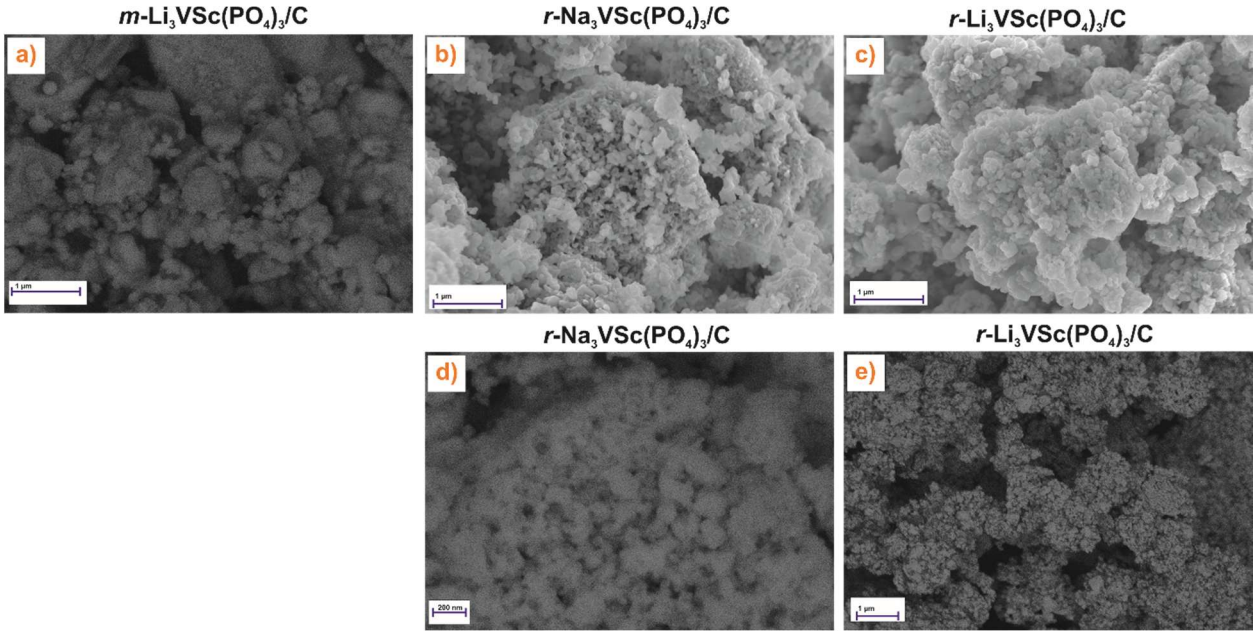


**Fig. S1.** SEM images of the *m*-LVScP/C material in ESB mode (a); SEM images of the $Na_3VSc(PO_4)_3$/C material (used as a precursor for the synthesis of *r*-LVScP/C by ion exchange) (b) and the resulting *r*-LVScP/C material (c), also in ESB mode (d, e respectively).

**Section 2.** Characterization of the chemical composition of *r*-LVScP.

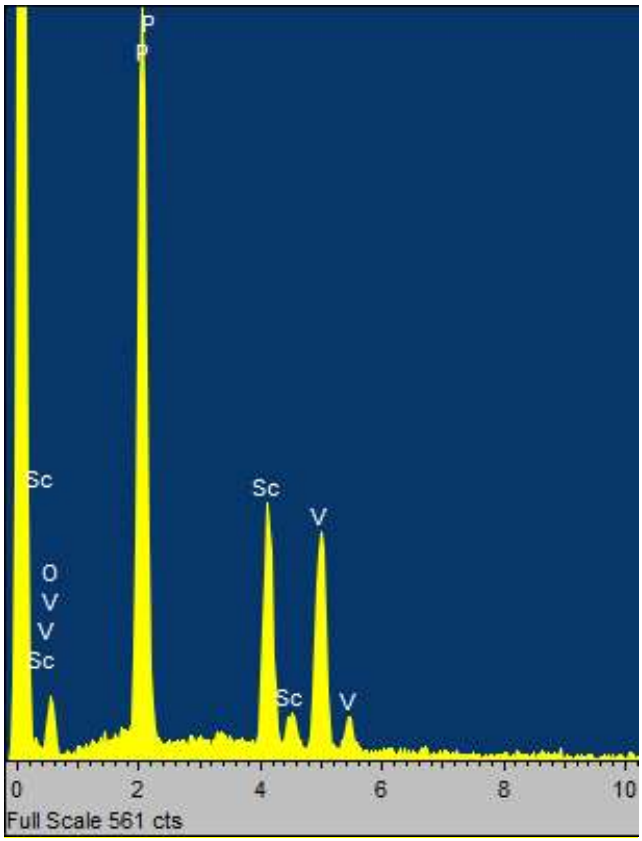


**Fig. S2.** EDX spectrum obtained for the *r*-LVScP/C sample prepared by $Li^+ \rightarrow Na^+$ ion exchange.

***Supplementary Note 1***. ICP-OES study of *r*-LVScP/C.

The weighted sample of 12.10 mg± 0.01 mg was placed in a glass triangle beaker (Erlenmeyer flask) of 100 ml, 10 ml of aqua conc. nitric ($HNO_3$) and 10 ml of conc. hydrochloric (HCl) acid (Panreac, Spain) was added. The sample was kept at ambient temperature until the complete release of $NO_x$ and material dissolution. A slightly green, transparent solution was obtained. Solution transferred to a volumetric flask (class A, 50.0 ml) and deionized water added to mark top-off. Before measurement, the solution was diluted 1000-fold.

An inductively coupled plasma atomic emission spectrometry (ICP–OES) Agilent 720 (Australia) was used. Argon gas was supplied using liquid argon (99.993% assay). All required parameters were optimized in this work before analysis (Table SI Note 1a.). Wavelengths' calibration and torch alignment were performed according to standard protocol. Optimization of measurement conditions was carried out in accordance with [https://doi.org/10.1016/j.aca.2026.345140].
The wavelengths used for analysis are given in the table. The Ni solution (20 mg/ml in 5 mass.% $HNO_3$) was used as an internal standard to improve the reproducibility of the results by in-line addition (Trident In-Line Reagent Additions Kits, Glass Expansion). The reference solutions with concentrations of 0.1–100 mg/L were prepared, base solution was $HNO_3$ (5 mass.%), the number of points for every regression was 10, $R^2 \geq 0.995$ for every curve. The reference multi-element standard (10 mg/ml, except lithium, which was 1 mg/ml) was used for laboratory quality control.

According to ICP-OES data, the ratio of cations ($n$=8, $P$=0.95) is $\mathbf{Li_{3.02 \pm 0.08}V_{1.00 \pm 0.03}Sc_{1.05 \pm 0.03}P_{2.96 \pm 0.07}}$. The weight contents of cations determined by ICP-OES are given in Table SI Note 1b.

Table SI Note 1a. ICP-OES operating parameters

| **Parameters** | **Values** |
|---|---|
| RF power, kW | 1.35 |
| Nebulizer gas (Ar) flow rate, L/min | 1.75 |
| | |
| Plasma gas (Ar) flow rate, L/min | 18.0 |
| Sample flow rate, rpm | 15 |
| Integration time, s | 35 |
| Replicates | 4 |
| **Used wavelength, nm** | |
| Li | 670.783 |
| Na | 588.995, 589.592; |
| V | 292.401, 289.265, 311.071; |
| Sc | 335.372, 361.383, 431.408; |
| P | 213.618, 214.914, 253.561 |
| Ni (as internal standard) | 231.604 |

Table SI Note 1b. Weight contents of cations.

| **Element** | **ω, wt.%** |
|---|---|
| Li | 4.06 ± 0.12 |
| V | 9.88 ± 0.30 |
| Sc | 8.95 ± 0.27 |
| P | 17.74 ± 0.53 |
| Na | <0.01 (100 mg/kg) |

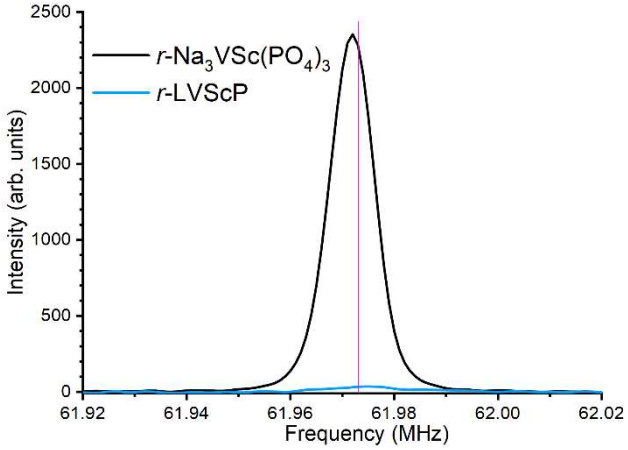


**Fig. S3.** Comparison of $^{23}$Na NMR spectra in the initial $Na_3VSc(PO_4)_3$/C material and after the ionic exchange procedure.

**Section 3**. Auxiliary data for crystal structure refinement.

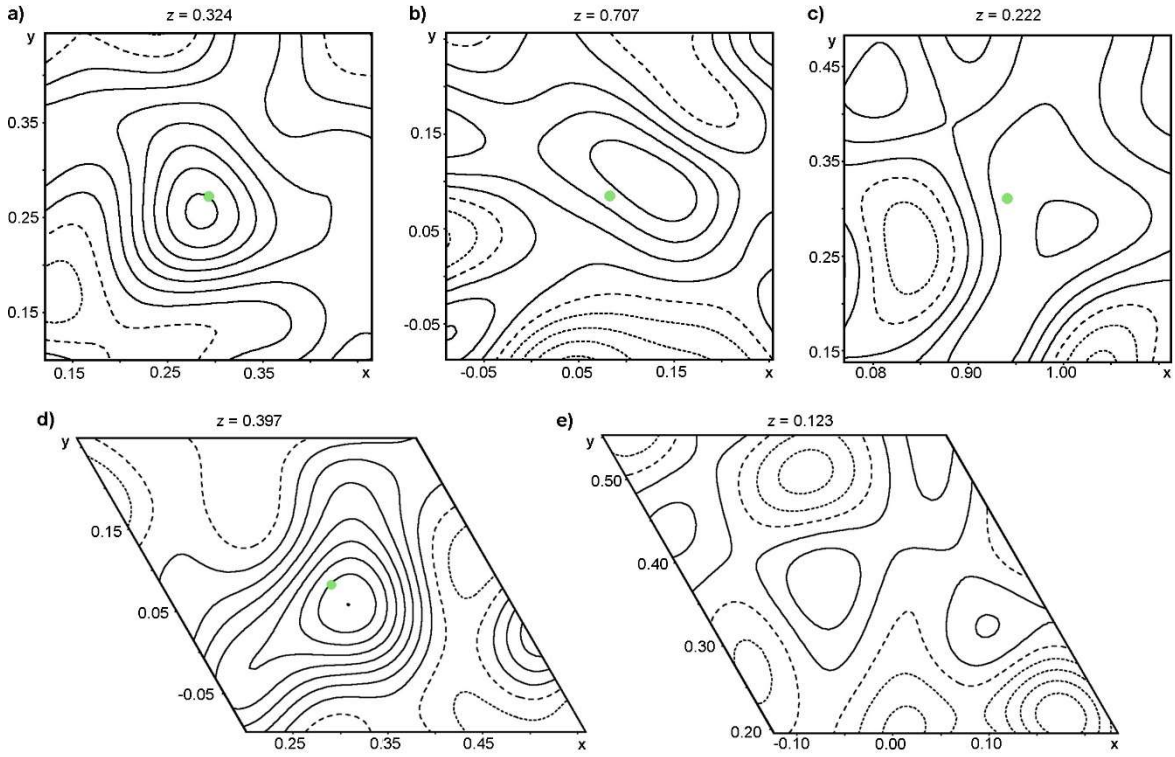


**Fig. S4**. Difference electron density map on (001)-plane corresponding to Li1 (a), Li2 (b) and Li3 (c) sites in the structure of *m*-LVScP; and to Li1 (d) site in the structure of *r*-LVScP. The highest residual positive maxima in the final difference Fourier synthesis for *r*-LVScP (e). The contour line is 0.05 *e*. The Li sites are marked by green circles. Real space fractional coordinates for the cross section are shown.

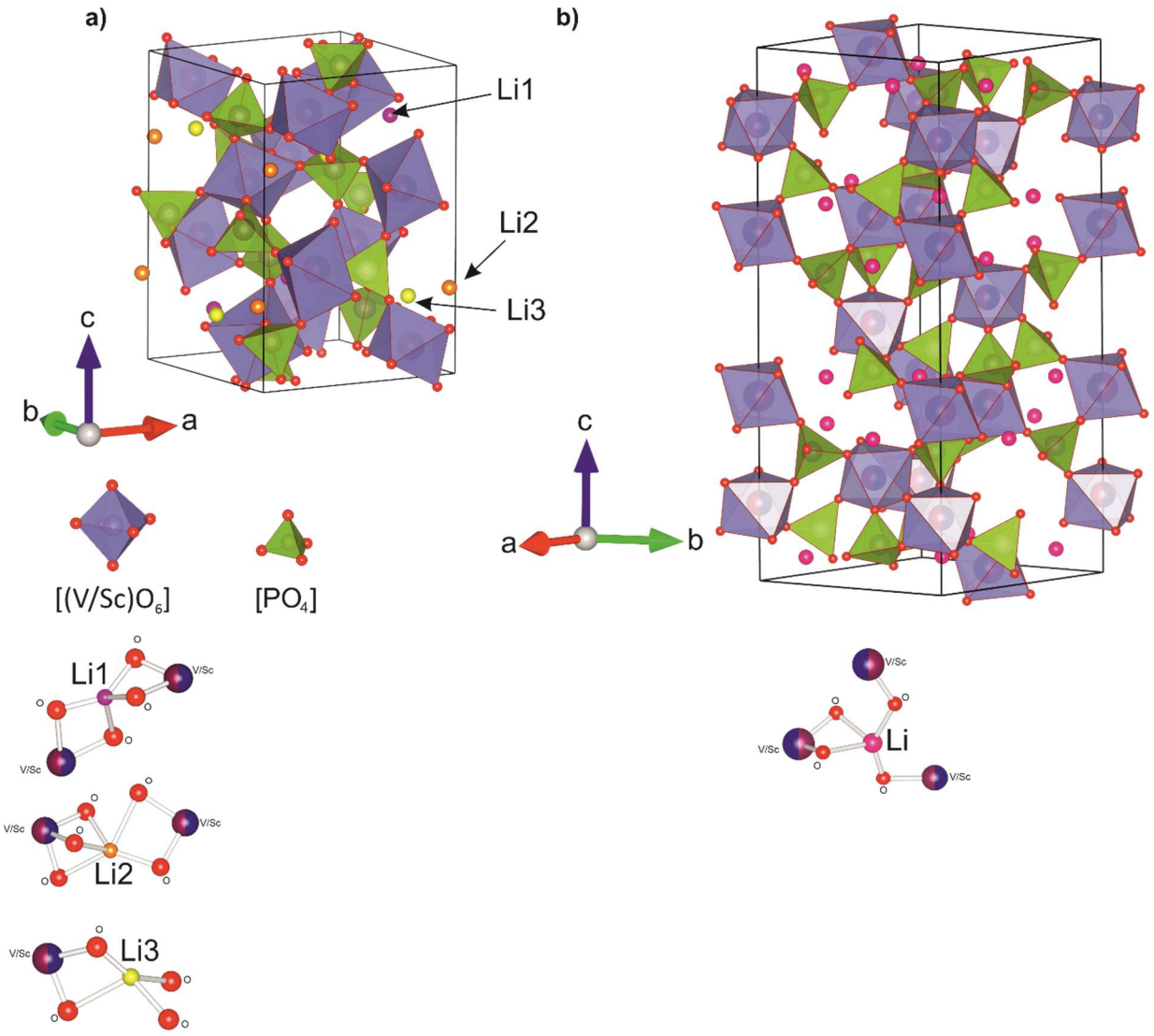


**Fig. S5**. Crystal structure and the environment of lithium atoms for *m*-LVScP (a) and *r*-LVScP (b).

**Section 4**. Electrochemical supplementary information.

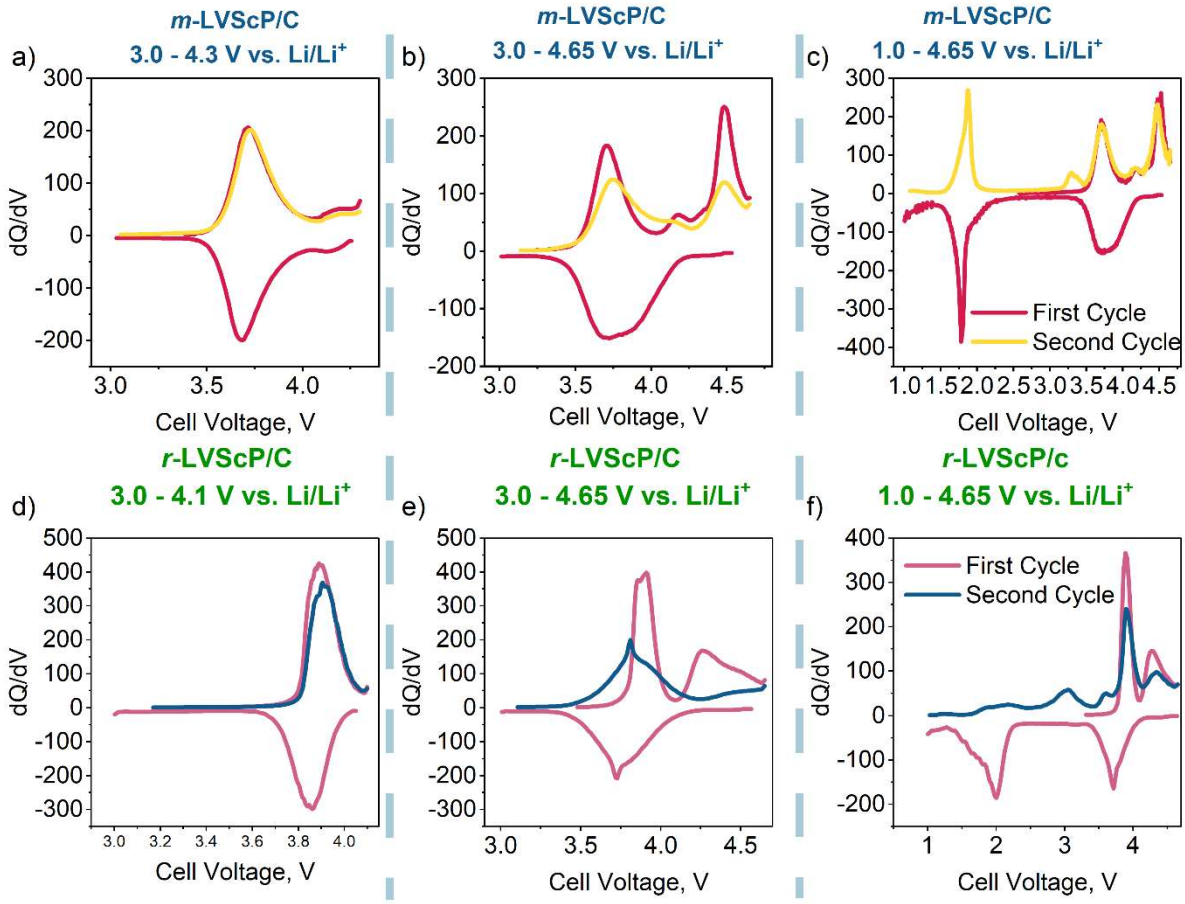


**Fig. S6**.dQ/dV plots of the first charge-discharge cycles for *m*-LVScP/C (a–c) and *r*-LVScP/C (d–f) materials in different potential ranges (vs. $Li/Li^+$).

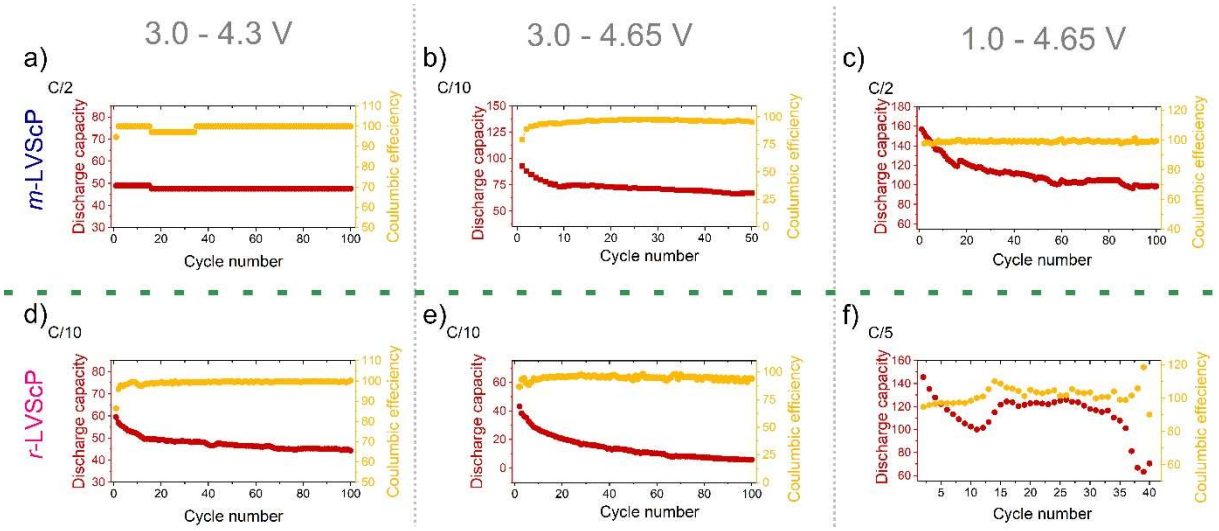


**Fig. S7**. The cycling performance of *m*-LVScP/C (a–c) and *r*-LVScP/C (d–f) materials in different potential ranges (vs. $Li/Li^+$).

**Section 5**. *Operando* PXRD.

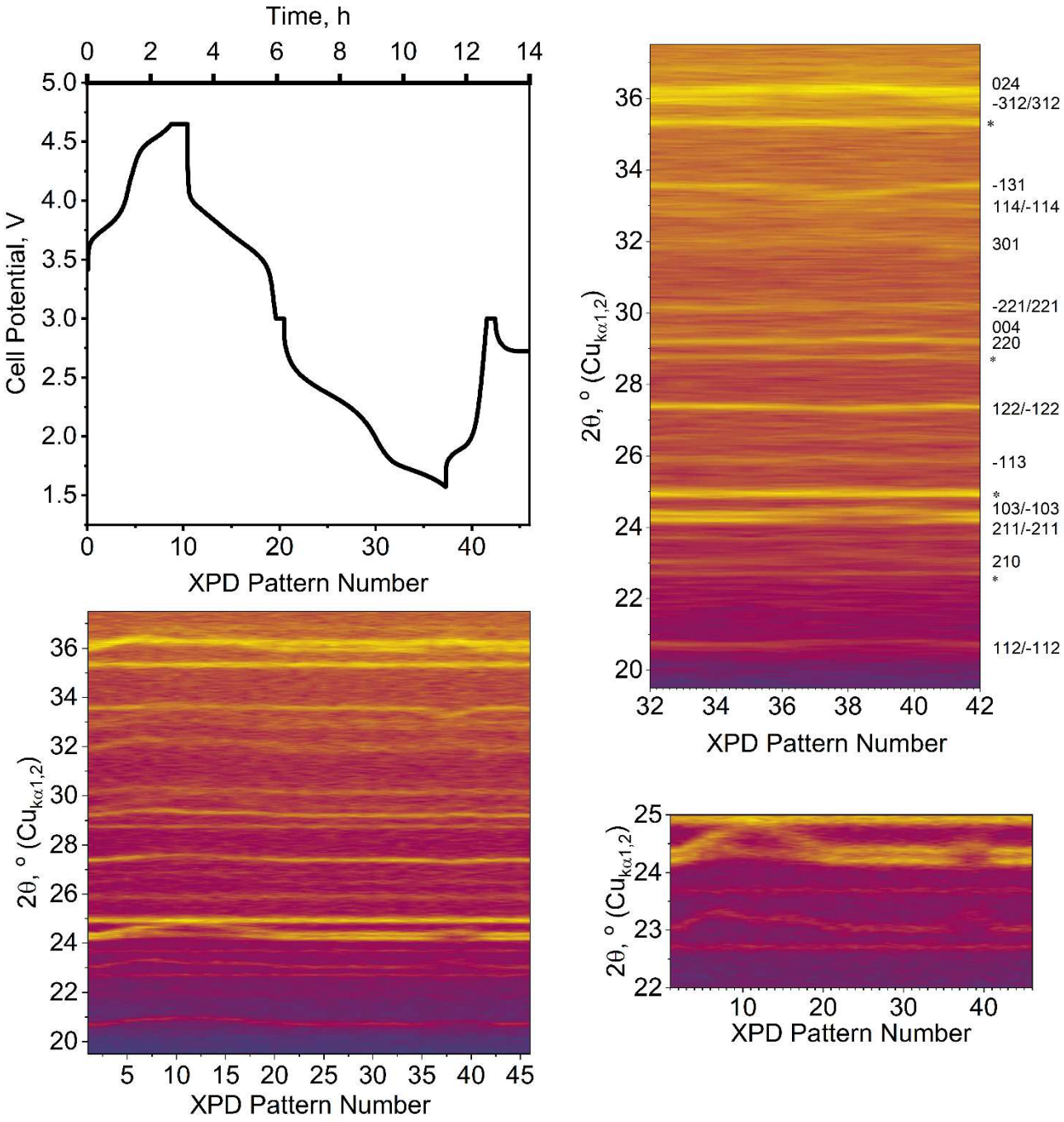


**Fig. S8.** The map of diffraction maxima for 20–37 °2θ region obtained during the first cycle for m-LVScP/C within the potential range of 3.5–4.65–1.5–3.5 V vs. Li/Li$^+$ at C/10 along with the corresponding charge-discharge curve. Two selected 2θ-regions are shown on the right at higher magnification. The lines of diffraction maxima are indexed in the right top image.

**Section 6**. *Ex situ* PXRD.

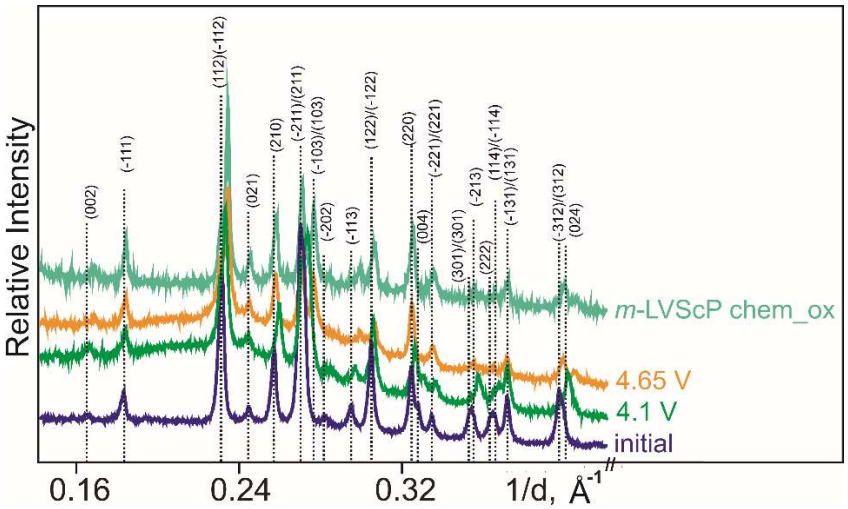


**Fig. S9.** A part of the *ex situ* PXRD patterns obtained for the *m*-LVScP/C electrodes at different states of charge (vs. $Li/Li^+$): an initial electrode (*blue*); an electrode charged to 4.1 V (*green*); an electrode charged to 4.65 V (*orange*) and for the chemically oxidized sample (*light green*).

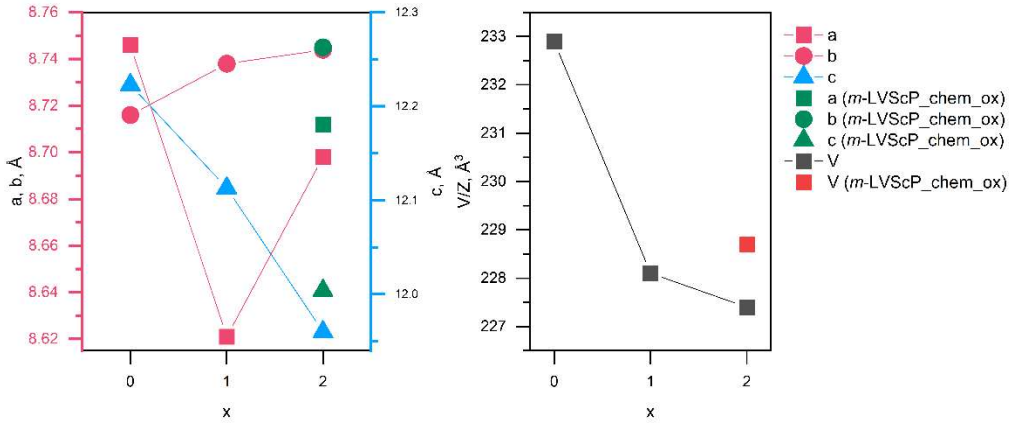


**Fig. S10.** Cell parameters ((*a, b, c*), a) and unit cell volumes per f.u. ((*V*/*Z*), b) determined for electrochemically and chemically synthesized *m*-$Li_{3-x}VSc(PO_4)_3$ phases ( $0 \le x \le 2$) as a function of *x*. The standard deviations are given in Table 2.

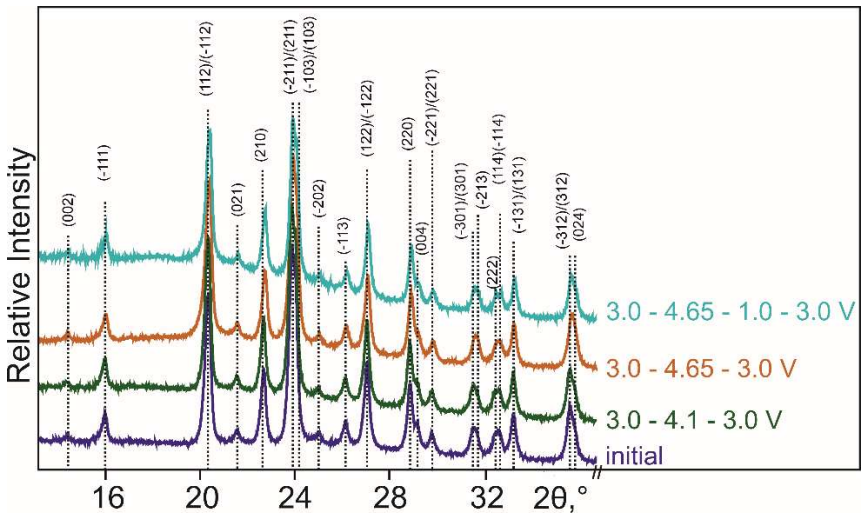


**Fig. S11.** A part of e*x-situ* PXRD patterns obtained for the *m*-LVScP/C electrodes at different states of charge (vs. $Li/Li^+$): an initial electrode (*violet*); an electrode after the first cycle within the range of 3.0–4.1 V (*green*); an electrode after the first cycle within the range of 3.0–4.65 V (*orange*); an electrode after the first cycle within the range of 1.0–4.65 V (*blue*).

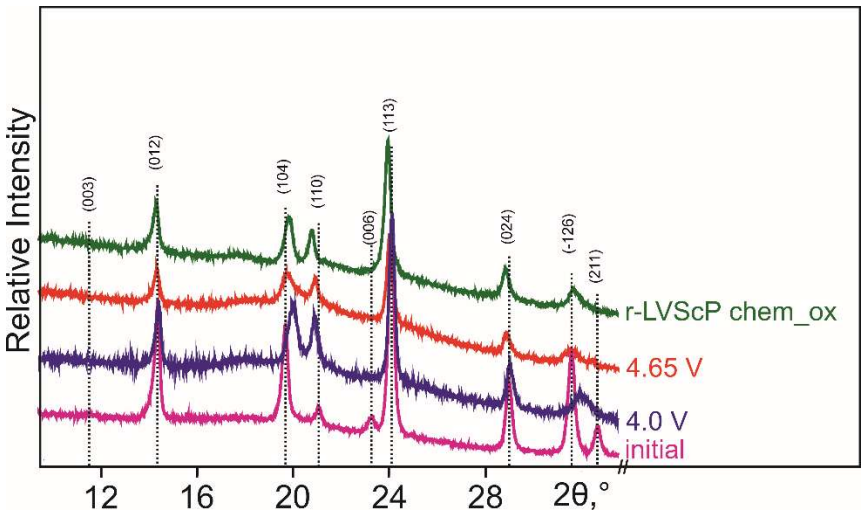


**Fig. S12.** A part of the *ex situ* PXRD patterns obtained for an initial electrode *r*-LVScP/C (*violet*), the electrodes charged to 4.0 V (*blue*) and 4.65 V (*red*) vs. $Li/Li^+$, and for the chemically oxidized sample (*green*).

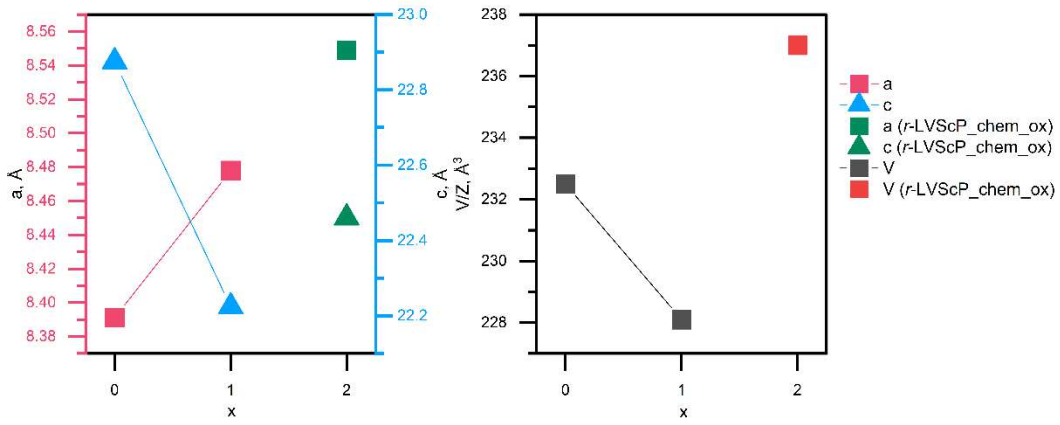


**Fig. S13.** Cell parameters ((*a, c*), a) and unit cell volumes per f.u. ((*V*/*Z*), b) determined for electrochemically and chemically synthesized *r*-$Li_{3-x}VSc(PO_4)_3$ phases ( $0 \le x \le 2$) as a function of *x*. The standard deviations are given in Table 2.

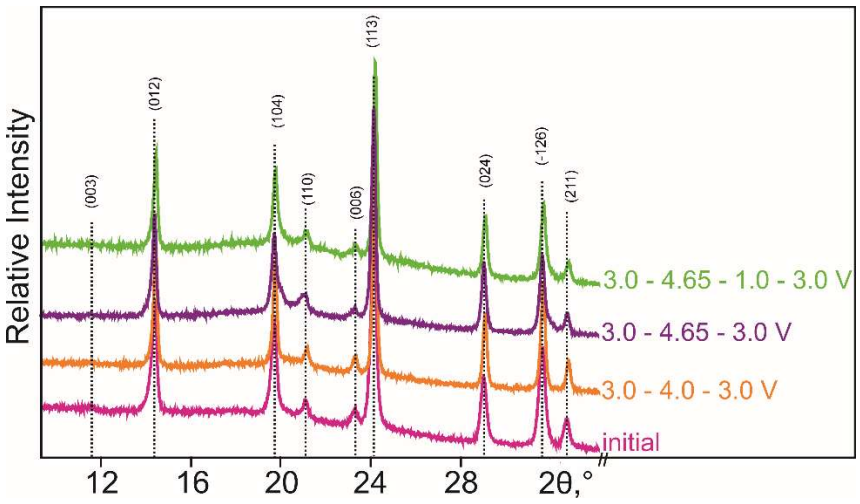


**Fig. S14.** A part of e*x-situ* PXRD patterns obtained for the *r*-LVScP/C electrodes at different states of charge (vs. $Li/Li^+$): an initial electrode (*pink*); an electrode after the first cycle within the range of 3.0–4.0 V (*orange*); an electrode after the first cycle within the range of 3.0–4.65 V (*violet*); an electrode after the first cycle within the range of 1.0–4.65 V (*green*).

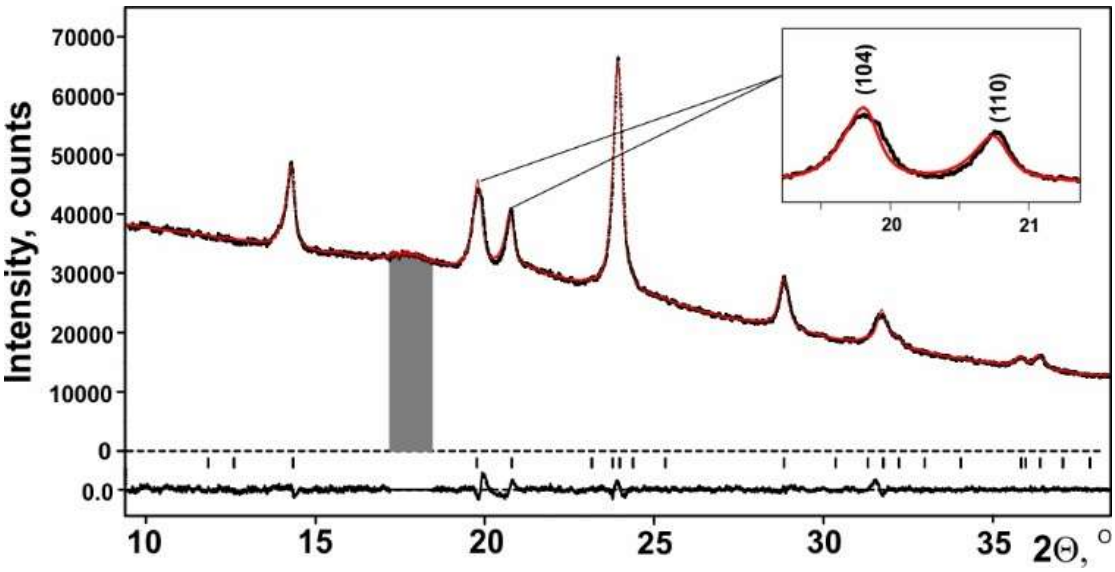


**Fig. S15.** Results of the full profile Le Bail fitting of the PXRD data of the chemically oxidized material *r*-LVScP_chem_ox. The insets show the fittings of the 104 and 110 maxima in detail. The PXRD pattern of *r*-LVScP_chem_ox can be indexed in rhombohedral symmetry, but the observed peak profile features for *r*-LVScP_chem_ox (e.g. for (104) reflection) may be treated as an evidence of the complex strain and/or slight distortion with symmetry reduction. It was the reason to compare the parameters in semi-quantitative manner, to define only trends in cell parameters variation.

**Section 7**. NMR study of *m*-LVScP/C and *r*-LVScP/C.

*Supplementary Note 2*. Additional NMR data for *m*-LVScP/C and *r*-LVScP/C.

The proposed in main text lithium arrangement is confirmed by the results of the study of the magnetization decay curve as a function of delay after the inversion pulse of $^{7}$Li nuclei in *m*-LVScP (Fig. S13a). The best fit of the curve corresponds to two exponential decays with a fixed amplitude ratio of 1:2. The existence of two different types of Li local surrounding in the structure of *r*-LVScP was also confirmed by magnetization decay curve of $^{7}$Li nuclei (Fig. S13b) where the best fit ratio of two $T_1$ components is 5.33 in excellent agreement with $^{7}$Li NMR spectrum (Fig. 6b).

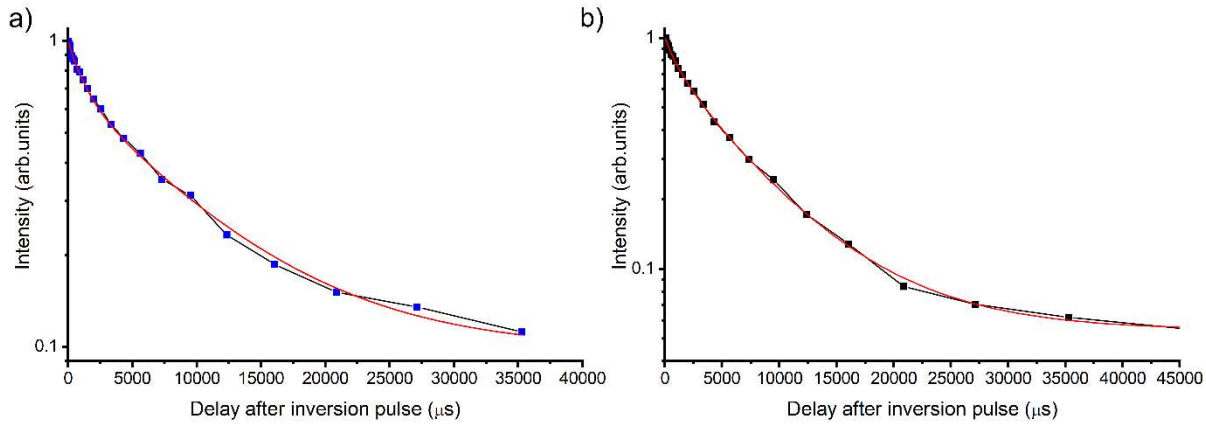


**Fig. S16.** Magnetization decay curve ($M_{echo} - M_{inv.echo}$) as a function of delay after inversion pulse of $^{7}$Li nuclei in *m*-LVScP (a) and *r*-LVScP (b). *Red solid line* is the best fit by two exponential decays with fixed amplitude ratio 1:2 for *m*-LVScP and 5.33:1 for *r*-LVScP.

**<u>$^{45}$Sc NMR spectra</u>** in NASICON-type frameworks before $Na_3VSc(PO_4)_3$ and after (*r*-LVScP) $Li^+ \rightarrow Na^+$ ion exchange are shown in Fig. S14a. The spectrum of the first compound is symmetrical and can be approximated by a single Gaussian line. The $Li^+ \rightarrow Na^+$ ion exchange leads to noticeable broadening of the spectrum and its shift to higher frequencies. The spectrum of *r*-LVScP is well approximated by two Gaussians of equal intensity with the parameters of one of the lines (position and width) fixed the same as for $Na_3VSc(PO_4)_3$. Corresponding magnetization decay curves of $^{45}$Sc nuclei obtained for $Na_3VSc(PO_4)_3$ and *r*-LVScP are in agreement with the suggested approximations (Fig. S14b). Magnetization decay curve of $^{45}$Sc nuclei in $Na_3VSc(PO_4)_3$ was successfully approximated by stretched exponential decay function (*green solid line*). Using of the stretched exponent is justified by statistics in local surrounding of Sc atoms leading to slight nonequivalence (disorder) of Sc positions. Indeed, such approximation demonstrates much better coincidence with the experimental points than the single exponential decay shown by the *blue solid*

*line*. Magnetization decay curve of $^{45}$Sc nuclei in *r*-LVScP is demonstrated in Fig. S14c. Two exponential decay function with equal amplitudes provides much better approximation (*red solid line*) than the single exponential decay (*blue solid line*).

The changes in the $^{45}$Sc NMR spectrum correlate with a strong distortion of the polyanion NASICON-framework, resulting in the disappearance of *c*-glide plane and splitting of the *B*-site.

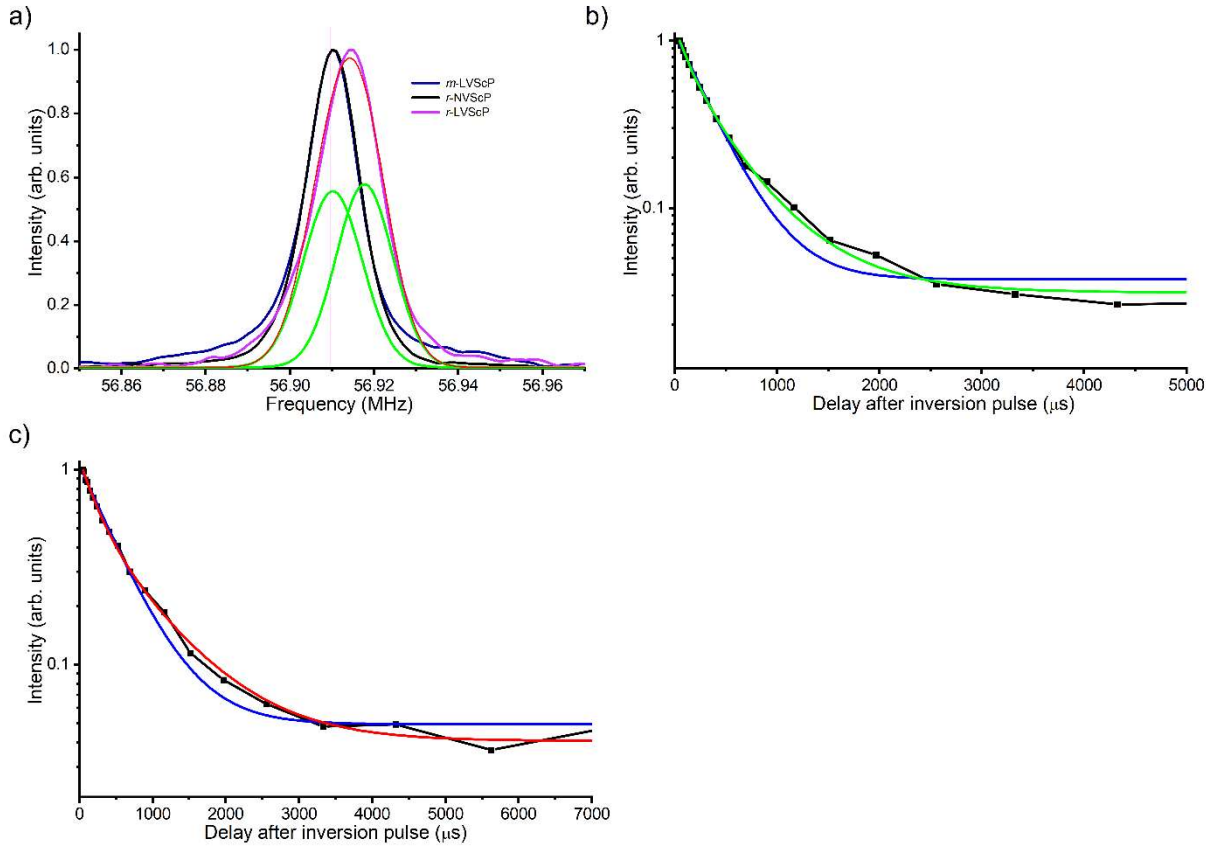


**Fig. S17.** (a) $^{45}$Sc NMR spectra of $Na_3VSc(PO_4)_3$ and *r*-LVScP. The spectrum of *r*-LVScP is approximated (*red solid line*) by two Gaussians of equal intensity (*green solid lines*) with the parameters (position and width) are fixed the same as for $Na_3VSc(PO_4)_3$. (b) Magnetization decay curve of $^{45}$Sc nuclei in $Na_3VSc(PO_4)_3$ approximated by stretched exponential decay function (*blue solid line*). (c) Magnetization decay curve of $^{45}$Sc nuclei in *r*-LVScP. Approximation by two exponential decay function with equal amplitudes (*red solid line*) and single exponential decay (*blue solid line*) is shown.

**Section 8**. Structure refinement and crystallographic data.

**Table S1.** Data collection and crystallographic parameters for *m*-$Li_3VSc(PO_4)_3$ and *r*-$Li_3VSc(PO_4)_3$.

| Chemical composition | *m*-$Li_3VSc(PO_4)_3$ | *r*-$Li_3VSc(PO_4)_3$ |
|---|---|---|
| Composition refined by the Rietveld method | $Li_3VSc(PO_4)_3$ | $Li_3VSc(PO_4)_3$ |
| Chemical formula weight | 401.6 | 401.6 |
| Space group (№) | $P2_1/n$ (№ 14) | $R\bar{3}$ (№ 148) |
| *a*, Å | 8.7432(1) | 8.3906(2) |
| *b*, Å | 8.7185(1) | |
| *c*, Å | 12.2207(1) | 22.8722(8) |
| $\beta$, ° | 90.061(3) | |
| *V*, Å$^3$ | 931.5(2) | 1394.5(1) |
| *Z* | 4 | 6 |
| Calculated density, g·cm$^{-3}$ | 2.86 | 2.88 |
| Radiation $\lambda$, Å | Cu$K_{\alpha1}$ | Co$K_{\alpha1}$ |
| Sin$\theta/\lambda$ range, Å$^{-1}$ | 0.0567–0.4382 | 0.0487–0.4282 |
| Absorption coefficient, cm$^{-1}$ | 20.64 | 31.241 |
| Number of points | 14980 | 7501 |
| Number of observed reflections | 214 | 164 |
| Refined parameters | 46 | 42 |
| $R_I$, $R_{wI}$ | 0.034, 0.050 | 0.042, 0.050 |
| $R_P$, $R_{wP}$ | 0.023, 0.030 | 0.048, 0.060 |
| GOF | 3.31 | 1.07 |

**Table S2.** Atomic coordinates and isotropic displacement parameters for *m*-$Li_3VSc(PO_4)_3$ (standard deviations are given without Berar factors).

| *Atom* | *Site* | *x/a* | *y/b* | *z/c* | *Occupancy* | $U_{iso}$[1)] , Å$^2$ |
|---|---|---|---|---|---|---|
| Li1[2)] | 4*e* | 0.2928 | 0.2722 | 0.3260 | 1 | 0.05 |
| Li2[2)] | 4*e* | 0.0821 | 0.0847 | 0.7072 | 1 | 0.05 |
| Li3[2)] | 4*e* | 0.9411 | 0.3103 | 0.2219 | 1 | 0.05 |
| *B*1[3)] | 4*e* | 0.2462(4) | 0.4669(3) | 0.1124(3) | 0.5V/0.5Sc | 0.006 |
| *B*2[3)] | 4*e* | 0.7544(4) | 0.4598(3) | 0.3906(3) | 0.5V/0.5Sc | 0.006 |
| P1[4)] | 4*e* | 0.1043(3) | 0.1047(4) | 0.1466(3) | 1 | 0.01 |
| P2[4)] | 4*e* | 0.6051(3) | 0.1078(4) | 0.3476(3) | 1 | 0.01 |
| P3[4)] | 4*e* | 0.0449(1) | 0.2496(5) | 0.4990(4) | 1 | 0.01 |
| O1 | 4*e* | 0.1394(7) | 0.0781(7) | 0.0253(3) | 1 | 0.01 |
| O2 | 4*e* | 0.1661(6) | 0.2586(7) | 0.1829(5) | 1 | 0.01 |
| O3 | 4*e* | 0.1800(6) | -0.0262(6) | 0.2144(4) | 1 | 0.01 |
| O4 | 4*e* | -0.0704(7) | 0.0955(7) | 0.1649(5) | 1 | 0.01 |
| O5 | 4*e* | 0.4308(4) | 0.1170(2) | 0.3570(5) | 1 | 0.01 |
| O6 | 4*e* | 0.650(2) | -0.0088(8) | 0.2612(5) | 1 | 0.01 |
| O7 | 4*e* | 0.6716(7) | 0.0596(7) | 0.4608(4) | 1 | 0.01 |
| O8 | 4*e* | 0.6694(1) | 0.268(1) | 0.3197(5) | 1 | 0.01 |
| O9 | 4*e* | 0.1623(8) | 0.1671(8) | 0.4271(6) | 1 | 0.01 |
| O10 | 4*e* | 0.1247(6) | 0.3580(9) | 0.5770(5) | 1 | 0.01 |
| O11 | 4*e* | -0.0465(6) | 0.1271(6) | 0.5645(5) | 1 | 0.01 |
| O12 | 4*e* | -0.0694(6) | 0.3372(8) | 0.4254(5) | 1 | 0.01 |

[1)] Atomic displacement parameters for all atoms have been fixed.

[2)] The coordinates, occupancies and ADPs of lithium sites Li1–Li3 have not been refined.

[3)] The *B*1 and *B*2 sites have been refined as statistically occupied by V and Sc in fixed atomic ratio 1 : 1.

[4)] Atomic coordinates of phosphorus and oxygens atoms have been refined using the rigid body model as tetrahedral blocks (P1)(O1)(O2)(O3)(O4), (P2)(O5)(O6)(O7)(O8) and (P3)(O9)(O10)(O11)(O12). The geometry of tetrahedral blocks have been taken from ICSD database (#167044) and fixed.

**Table S3**. Selected interatomic distances in *m*-$Li_3VSc(PO_4)_3$.

| *Atoms* | *Distance*, Å | *Atoms* | *Distance*, Å | *Atoms* | *Distance*, Å |
|---|---|---|---|---|---|
| Li1−O5 | 1.85(1) | *B*1−O7 | 1.977(6) | P1−O2 | 1.513(7) |
| O3 | 1.841(5) | O9 | 1.980(7) | O1 | 1.531(6) |
| O9 | 1.916(7) | O5 | 2.059(11) | O3 | 1.558(6) |
| O2 | 2.072(6) | O11 | 2.072(6) | O4 | 1.546(6) |
| Li2−O8 | 2.028(8) | O2 | 2.129(7) | P2−O6 | 1.513(8) |
| O11 | 2.109(6) | O3 | 2.214(6) | O7 | 1.531(5) |
| O4 | 2.218(6) | *B*2−O12 | 1.922(7) | O7 | 1.558(6) |
| O6 | 2.47(1) | O10 | 1.948(8) | O8 | 1.546(10) |
| O3 | 2.536(5) | O1 | 1.958(6) | P3−O10 | 1.513(8) |
| Li3−O6 | 1.785(9) | O8 | 2.022(1) | O9 | 1.531 (8) |
| O4 | 2.001(6) | O6 | 2.055(9) | O11 | 1.558(7) |
| O2 | 2.075(6) | O12 | 2.109(7) | O12 | 1.546(7) |
| O12 | 2.499(6) | | | | |

**Table S4.** Atomic coordinates and isotropic displacement parameters for *r*-$Li_3VSc(PO_4)_3$ (standard deviations are given without Berar factors).

| *Atom* | *Site* | *x/a* | *y/b* | *z/c* | *Occupancy* | $U_{iso}$, Å$^2$ |
|---|---|---|---|---|---|---|
| Li1 | 18*f* | 0.380(5) | 0.082(4) | 0.387(1) | 1 | 0.053(14) |
| *B*1[1)] | 6*c* | 0 | 0 | 0.1457(4) | 0.5V/0.5Sc | 0.006(3) |
| *B*2[1)] | 6*c* | 0 | 0 | 0.6537(4) | 0.5V/0.5Sc | 0.016(3) |
| P[2)] | 18*f* | 0.2917(4) | -0.0018(7) | 0.2503(2) | 1 | 0.019(2) |
| O1[2)] | 18*f* | 0.1913(11) | -0.0185(13) | 0.1918(3) | 1 | 0.032(2)[3)] |
| O2 | 18*f* | 0.2375(10) | 0.0901(12) | 0.2976(3) | 1 | 0.032(2) |
| O3 | 18*f* | 0.2408(10) | -0.2005(9) | 0.2673(4) | 1 | 0.032(2) |
| O4 | 18*f* | 0.4971(8) | 0.1119(12) | 0.2429(5) | 1 | 0.032(2) |

[1)] The *B*1 and *B*2 sites have been refined as statistically occupied by V and Sc in fixed atomic ratio 1:1.

[2)] Atomic coordinates of phosphorus and oxygens atoms have been refined using the rigid body model as tetrahedral block. The geometry of tetrahedral blocks have been taken from ICSD database (#167044) and fixed.

[3)] The ADPs of the oxygen atoms have been constrained.

**Table S5.** Selected interatomic distances in *r*-$Li_3VSc(PO_4)_3$.

| *Atoms* | *Distance*, Å | *Atoms* | *Distance*, Å | *Atoms* | *Distance*, Å |
|---|---|---|---|---|---|
| Li1−O4 | 1.70(4) | *B*1−O1 | 1.99(1) × 3 | P−O4 | 1.505(7) |
| O3 | 2.10(5) | O4 | 2.10(1) × 3 | O2 | 1.524(10) |
| O2 | 2.19(3) | *B*2−O2 | 2.05(1) × 3 | O3 | 1.549(9) |
| O2 | 2.38(4) | O3 | 2.07(1) × 3 | O1 | 1.551(8) |